

## Supporting Information

### Experimental Section

#### Materials

Ammonium metavanadate ( $\text{NH}_4\text{VO}_3$ ) was purchased from Shanghai Aladdin Biochemical Technology Co. Ltd. Aniline (AI) was purchased from Shanghai Adama Beta Chemical Reagent Co. Ltd. Oxalic acid was purchased from Shanghai Aladdin Biochemical Technology Co. Ltd. Glass fiber membrane (GF/D grade) was provided by Whatman company. Zinc foil (diameter: 15 mm, thickness: 0.3 mm) was purchased from Dongguan Keloude Experimental Materials Technology Co. Ltd. Titanium foil (diameter: 15 mm, thickness: 0.1 mm) was purchased from Guangzhou Haiyuan Metal Products Co. Ltd. Conductive carbon black (Super P Li) was purchased from Guangdong Candlelight New Energy Technology Co. Ltd. Polyvinylidene fluoride (PVDF) was purchased from Wuyu Chemical Industry Co. Ltd. Zinc trifluoromethylsulfonate ( $\text{Zn}(\text{CF}_3\text{SO}_3)_2$ ) was purchased from Shanghai McLean Biochemical Technology Co. Ltd.

#### Synthesis of NVO and NVO/PANI

NVO and NVO/PANI were synthesized by one-step solvothermal method. 2.4 mmol dihydrate oxalic acid, 0.5 mmol aniline and 40 ml of deionized water were mixed and ultrasound for 30 minutes, then 2 mmol ammonium metavanadate was added and further stirred for 30 minutes. The solution was sealed in a 50 mL autoclave and heated to 180 °C for 8 h. The NVO/PANI was collected by filtering, washing (deionized water

and ethanol) and drying (60°C for 8 h). Under the same conditions, NVO was prepared without adding aniline.

### **Characterizations**

The crystal structure of the sample was obtained by the radiation X-ray diffractometer (XRD, Japan Science, SmartLab3), and the Fourier infrared spectrum (FTIR) came from the infrared spectrometer (ThermoFisher Nicolet iS-10). Scanning electron microscopy (SEM) and energy dispersive X-ray spectroscopy (EDS) mapping images of the samples were obtained by J Hitachi S-4800 instrument equipped with an EDS (AMETEK) analyzer at an accelerated voltage of 3 kV. X-ray photoelectron spectroscopy (XPS) analysis was performed on the Thermo ESCALAB 250 X-ray photoelectron spectrometer. Electron paramagnetic resonance (EPR) spectroscopy was performed using an EPR (BRUKE EMXPLUS) with a central field of 3600 G and a scanning width of 100G. Nitrogen (N<sub>2</sub>) adsorption-desorption curves were measured by a 3Flex three-station universal gas adsorbent (Micromeritics, USA). Thermogravimetric (TG) curves were measured from 50 °C to 800 °C in N<sub>2</sub> atmosphere by TGA/SDTA851E (Mettler Toledo). The Raman spectrum is measured by a Horiba Scientific LabRAM HR Evolution equipped with a 633 nm He Ne laser. The pore volume and specific surface area were measured by Brunauer-Emmet Teller (BET) surface analyzer (Micromeritics, ASAP 2020). All cyclic voltammetric tests (CV) and electrochemical impedance spectroscopy (EIS) were obtained using CHI760E electrochemical workstation (Chenhua, Shanghai, China). EIS was performed with an AC amplitude voltage of 5 mV in the frequency range of 0.01 Hz~100 kHz. The

constant current charge/discharge (GCD) test with voltage range of 0.1 V to 1.6 V was conducted on LAND CT2001A (5 V/5 mA).

### **Battery fabrication**

All samples (NVO and NVO/PANI) are mixed with Super P Li and PVDF at the ratio of 6:3:1, then NMP is added and fully milled, the resulting slurry is coated on titanium foil, and dried in vacuum at 60 °C for 8 h. The average mass loading is kept in the range of 1.0-1.5 mg cm<sup>-2</sup>. The CR2032 button battery is used, and the assembly process is in air atmosphere (Zinc foil as anode; glass fiber as separator), with 80 μL 3 M Zn(CF<sub>3</sub>SO<sub>3</sub>)<sub>2</sub> as aqueous electrolyte. All fabricated batteries were stood at room temperature for 12 h before the electrochemical test.

### **Density functional theory (DFT) calculations**

We have utilized the Vienna Ab Initio Package (VASP)<sup>[1,2]</sup> to carry out all spin-polarized density functional theory (DFT) computations within the generalized gradient approximation (GGA) by employing the Perdew-Burke-Ernzerhof (PBE)<sup>[3]</sup> formulation. We have elected the projected augmented wave (PAW) potentials<sup>[4,5]</sup> for depicting the ionic cores and taken valence electrons into account through a plane wave basis set with a kinetic energy cutoff of 450 eV. Partial occupancies of the Kohn–Sham orbitals were permitted using the Gaussian smearing method with a width of 0.05 eV. The electronic energy was regarded as self-consistent when the energy change was less than 10<sup>-5</sup> eV. A geometry optimization was deemed convergent when the energy change was smaller than 0.02 eV Å<sup>-1</sup>. The vacuum spacing in a direction perpendicular to the plane of the structure is 18 Å. The weak interaction was described by the DFT +

D3 method via empirical correction in Grimme's scheme<sup>[6, 7]</sup>.

The bind energy ( $E_b$ ) has been calculated using Eq. 1,

$$E_b = E_{\text{total}} - E_{\text{substrate}} - E_{\text{Zn}} \quad (1)$$

The  $E_{\text{total}}$ ,  $E_{\text{substrate}}$  and  $E_{\text{Zn}}$  respectively represent the energy of the structure with Zn atom, substrate without a Zn atom and a Zn atom in the adsorption structure.

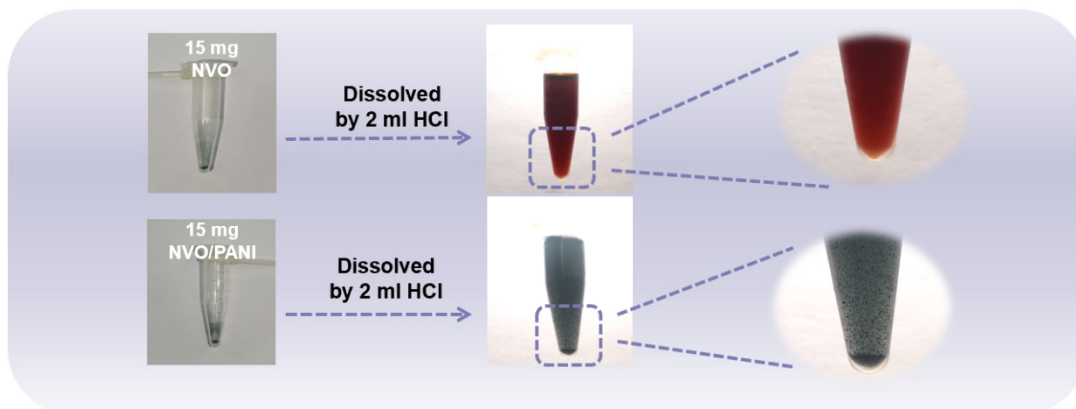


**Fig. S1** Hydrochloric acid treated NVO, NVO/PANI.

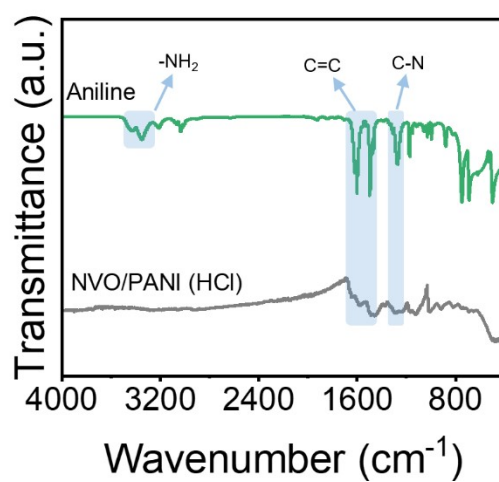


**Fig. S2** FTIR spectra of aniline and NVO/PANI treated with hydrochloric acid.

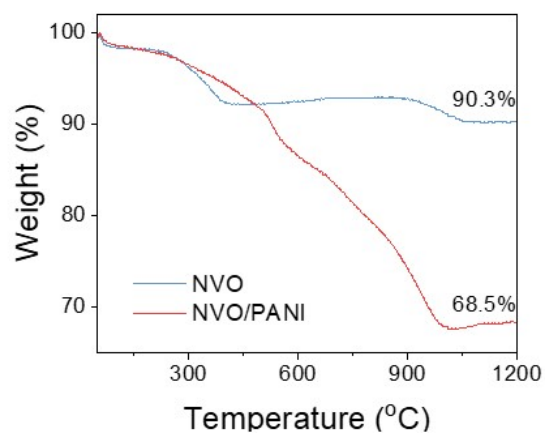


**Fig. S3** TGA curves of NVO and NVO/PANI.

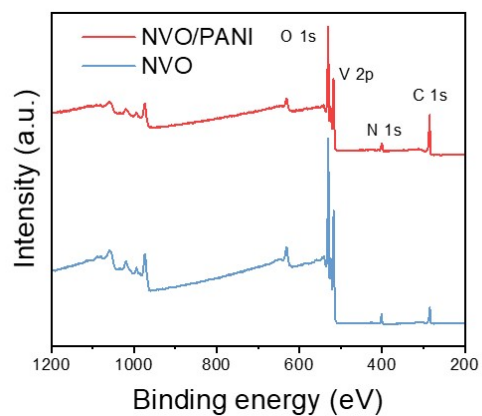


**Fig. S4** Survey XPS spectra of NVO, NVO-PANI.

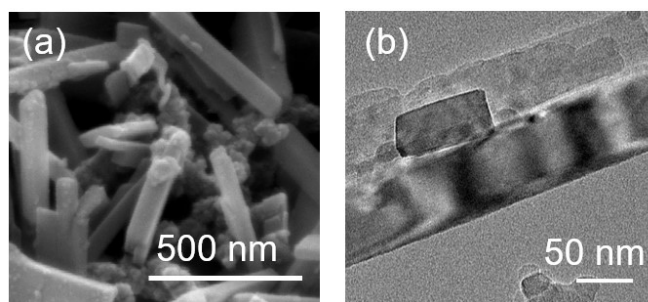


**Fig. S5** (a) SEM and (b) TEM images of NVO/PANI

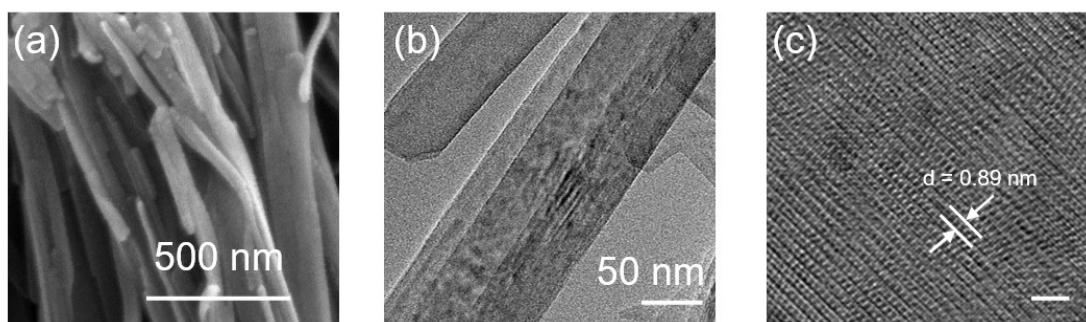


**Fig. S6** (a) SEM, (b) TEM and (c) HRTEM of NVO

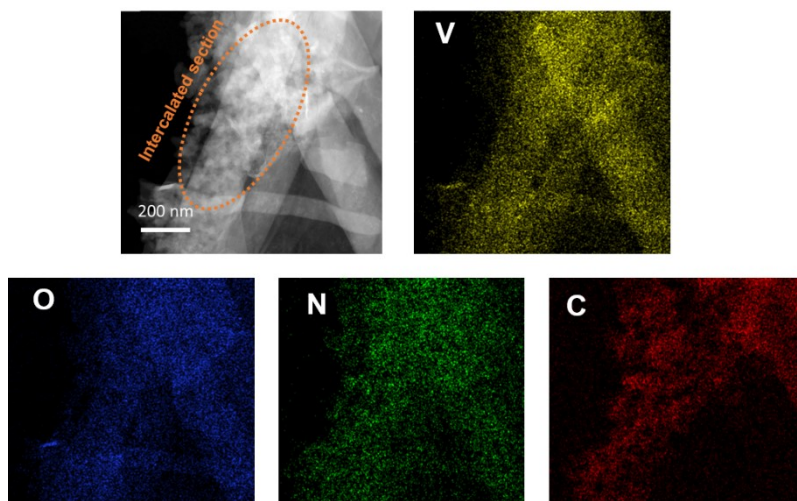


**Fig. S7** TEM-EDS elemental mapping of NVO/PANI.

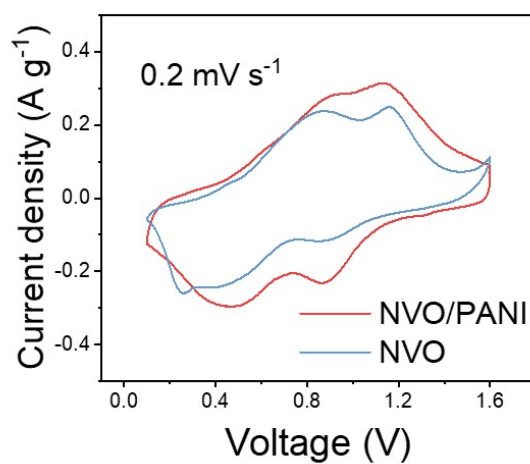


**Fig. S8** CV curves of NVO and NVO/PANI cathodes at  $0.2 \text{ mV s}^{-1}$ .

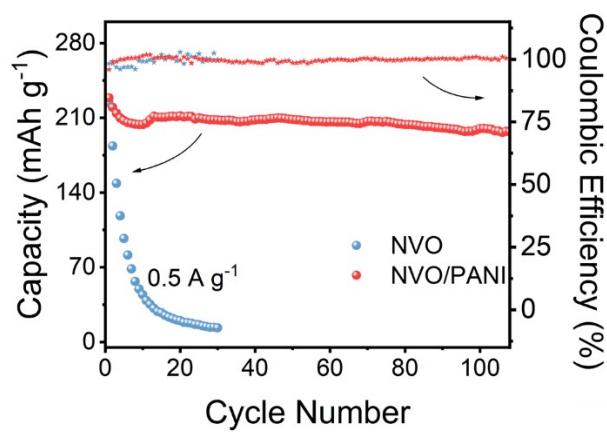


**Fig. S9** Cycle performance of NVO and NVO/PANI cathodes at  $0.5 \text{ A g}^{-1}$ .

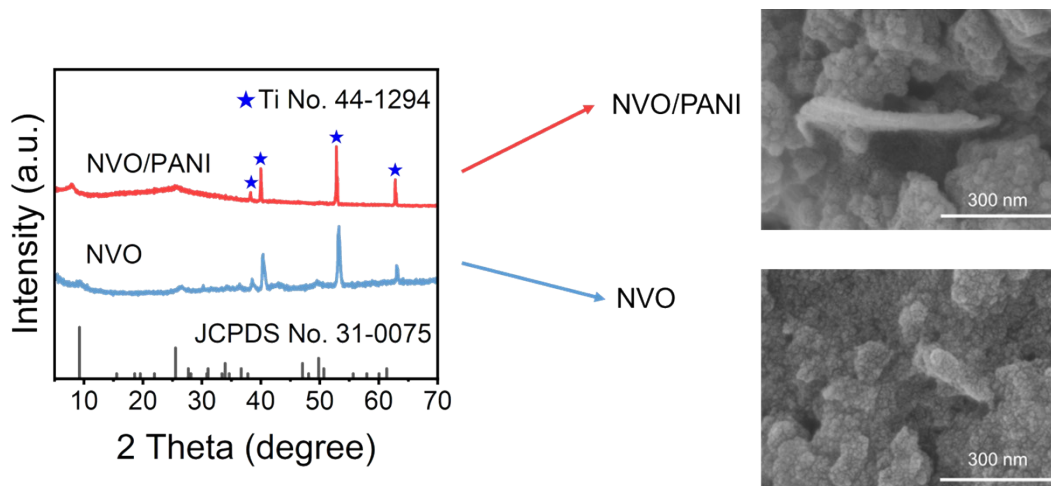


**Fig. S10** The XRD patterns and SEM images of NVO and NVO/PANI cathodes after 500 cycles.

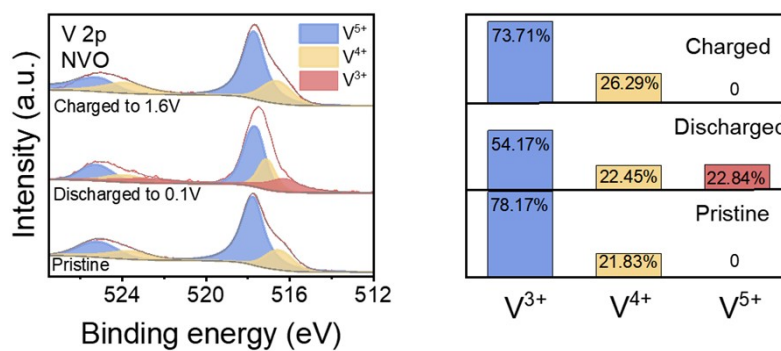


**Fig. S11** Ex-situ XPS of V 2p for NVO cathode at different GCD states, together with corresponding ratios

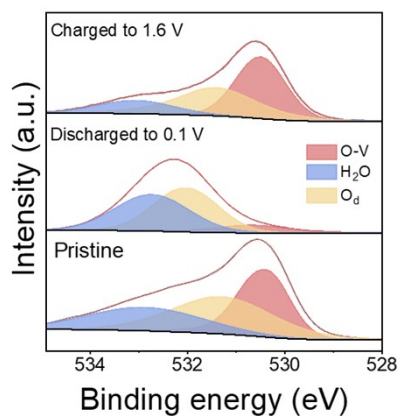


**Fig. S12** High resolution XPS spectra of O 1s for NVO/PANI.



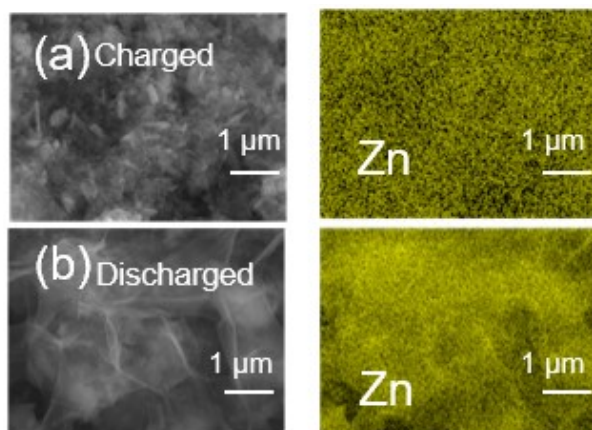


**Fig. S13** EDS mapping of Zn element for NVO/PANI capture in ZIB at different GCD states.

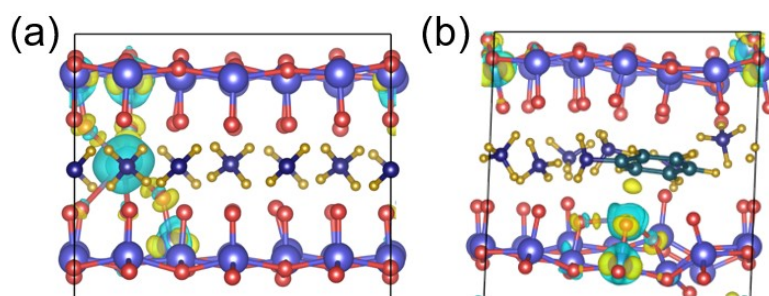


**Fig. S14** Charge density of (a) NVO and (b) NVO/PANI with  $Zn^{2+}$  ions intercalation

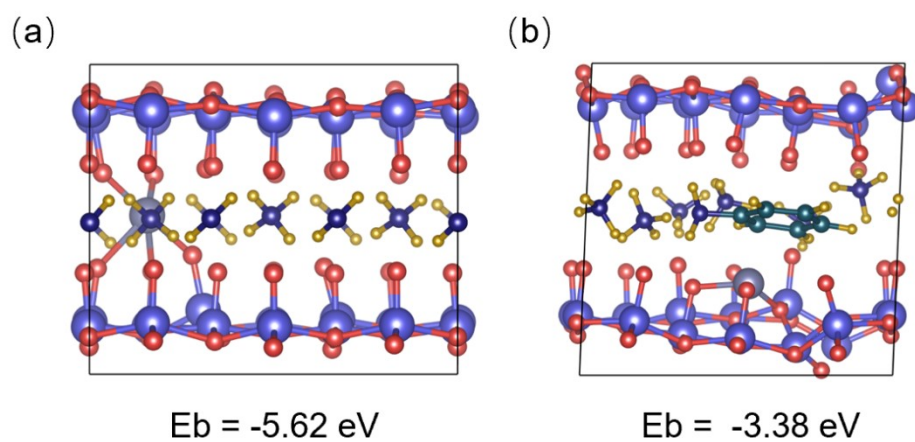


**Fig. S15** Calculation model with Zn-ion intercalation in (a) NVO and (b) NVO/PANI.

## References:

1. Kresse, G.; Furthmüller, J. *Comput. Mater. Sci.* 1996, 6, 15-50.
2. Kresse, G.; Furthmüller, J. *Phys. Rev. B* 1996, 54, 11169-11186.
3. Perdew, J. P.; Burke, K.; Ernzerhof, M. Generalized Gradient Approximation Made Simple. *Phys. Rev. Lett.* 1996, 77, 3865-3868.
4. Kresse, G.; Joubert, D. From Ultrasoft Pseudopotentials to the Projector Augmented-Wave Method. *Phys. Rev. B* 1999, 59, 1758-1775.
5. Blöchl, P. E. Projector Augmented-Wave Method. *Phys. Rev. B* 1994, 50, 17953-17979.
6. S. Grimme, J. Antony, S. Ehrlich, and S. Krieg, *J. Chem. Phys.* 2010, 132, 154104.
7. S. Grimme, S. Ehrlich, and L. Goerigk, *J. Comp. Chem.* 2011, 32, 1456.